Dissociation of H_2 on Mg-coated $B_{12}C_6N_6$*

Li Ma(马丽), Xue-Ling Jin(金雪玲), Hui-Hui Yang(杨慧慧),
Xiao-Xia Wang(王小霞), Ning Du(杜宁), and Hong-Shan Chen(陈宏善)†

College of Physics and Electronic Engineering, Northwest Normal University, Lanzhou 730070, *China*

(Received 17 January 2017; revised manuscript received 25 March 2017; published online 10 May 2017)

The dissociation of H_2 molecule is the first step for chemical storage of hydrogen, and the energy barrier of the dissociation is the key factor to determine the kinetics of the regeneration of the storage material. In this paper, we investigate the hydrogen adsorption and dissociation on Mg-coated $B_{12}C_6N_6$. The $B_{12}C_6N_6$ is an electron deficient fullerene, and Mg atoms can be strongly bound to this cage by donating their valance electrons to the virtual 2p orbitals of carbon in the cluster. The preferred binding sites for Mg atoms are the B_2C_2 tetragonal rings. The positive charge quantity on the Mg atom is 1.50 when a single Mg atom is coated on a B_2C_2 ring. The stable dissociation products are determined and the dissociation processes are traced. Strong orbital interaction between the hydrogen and the cluster occurs in the process of dissociation, and H_2 molecule can be easily dissociated. We present four dissociation paths, and the lowest energy barrier is only 0.11 eV, which means that the dissociation can take place at ambient temperature.

Keywords: Mg-coated $B_{12}C_6N_6$, H_2 dissociation, energy barrier

PACS: 88.30.R–, 36.40.–c, 31.15.A–, 33.15.Fm **DOI:** 10.1088/1674-1056/26/6/068801

1. Introduction

The extensive consumption of fossil fuels leads to rapid depletion of these resources, and it also poses serious environmental pollution and threats our living environment. Providing an abundant, clean, and secure renewable energy source is one of the key technological challenges facing mankind. Hydrogen is potentially an ideal energy carrier, as it has the highest heating value per mass and the combustion produces only water.[1–5] However, a number of challenges must be overcome before hydrogen can be used broadly as a sustainable energy resource. Besides economic and high-performance means for large-scale hydrogen production, a safe and efficient storage medium is a crucial prerequisite for hydrogen serving as an energy carrier that can be realized, especially for the applications in the vehicles.[6–8] Solid state storage of hydrogen is superior due to its storage capacity (both gravimetric and volumetric), energy efficiency, and safety.[9–15] Developing compact hydrogen storage systems with proper kinetics is the most demanding and challenging part of realizing the hydrogen economy, and it attracts extensive efforts worldwide. Solid state hydrogen storage can be roughly divided into physisorption and chemisorption. In physisorption, molecular hydrogen is adsorbed on the surface or in the internal volume of porous materials by weak van der Waals interactions. In chemisorption, atomic hydrogen is chemically bound in the bulk of the material and the dissociation of hydrogen molecule is the first step which occurs usually at higher temperature. Developing materials with high recycling capacity and suitable uptake-release kinetics is still a great challenge. The technical targets set by the US Department of Energy for 2020 are 5.5% gravimetric density at operating temperatures $-40\ ^\circ\text{C}\sim 60\ ^\circ\text{C}$ with a charging/discharging rate of 1.5-kg H_2/min. To date, no systems have been found to reach a satisfactory level of performance because hydrogen molecules interact either too weakly (physisorption) or too strongly (chemisorption) with the host materials.

Magnesium hydride MgH_2 is an interesting candidate for onboard hydrogen storage due to its low atomic weight, high hydrogen storage capacity and low cost.[16–18] Although MgH_2 has a high gravimetric capacity of 7.6 wt%, it suffers slow kinetics and a high decomposition temperature; an equilibrium pressure of 0.1 MPa requires temperature about 300 °C.[17,18] Extensive investigations have been devoted to MgH_2 in the past 20 years to improve the kinetics of the absorption and desorption of hydrogen and cycle stability.[16–24] Particle size reduction by ball milling, alloying or doping are among the most common approaches that are being pursued to speed up the kinetics in the Mg–H systems.[20–22] Catalytically enhanced systems show great promise for improved hydrogen storage properties.[23,24] The recent focus of developing hydrogen storage materials has been shifted to metal decorated nanostructures. Previous studies indicated that capping metal atoms on carbon or BN systems could considerably increase hydrogen uptake due to the enhanced adsorption energy of H_2 on the positively charged metal atoms.[25–31] Unfortunately, transition metal atoms basically prefer being aggregated to being dispersed on the substrate because of the large cohesive energy of bulk transition metal. In this regard, coating alkali and alkaline-earth metal atoms are a better choice since their cohesive energies are much smaller.

The stability of $B_{12}C_6N_6$ is comparable to the pure carbon

*Project supported by the National Natural Science Foundation of China (Grant Nos. 11164024 and 11164034).
†Corresponding author. E-mail: chenhs@nwnu.edu.cn
© 2017 Chinese Physical Society and IOP Publishing Ltd

or boron nitride counterparts.[32] Our recent studies showed that the physical adsorption of H_2 molecule on $B_{12}C_6N_6$ is weak but the H_2 molecules can be easily dissociated on this cage; the dissociation energy barrier is only 0.35 eV.[33] As an electron deficient fullerene, part of the 2p orbitals of carbon in $B_{12}C_6N_6$ are unoccupied. It is anticipated that the metal atoms coated on this cage will transfer their valence electrons easily to the cluster and form states with large positive charges. In this paper, we use density functional theory calculations to explore the dissociation of H_2 on Mg-coated $B_{12}C_6N_6$ clusters. The results show that H_2 molecule can be easily dissociated on Mg-coated $B_{12}C_6N_6$. The lowest dissociation energy barrier is only 0.11 eV, which indicates that the dissociation can occur at ambient temperature.

2. Computational methods

The geometry optimization and energy calculation for the Mg-coated clusters and the H_2 adsorbed or dissociated systems are carried out by using the density functional theory with Becke's three-parameter exchange functional and Lee–Yang–Parr correlation functional (B3LYP).[34,35] The double-ζ split basis sets with polarization functions 6-31G(d,p) are employed. Vibrational frequencies are computed to make sure the optimized structures are of energy minima. All the computations are performed by using Gaussian 09 program.[36] The charge distribution is analyzed by the natural bond orbitals (NBOs)[37] and atoms in molecule (AIM)[38] model. The density of states (DOS) is calculated using the Multiwfn program.[39]

3. Results and discussion

3.1. Geometries and electronic structures of $B_{12}C_6N_6$

The structures of $B_{12}C_6N_6$ are generated by substituting six nitrogen atoms with six carbon atoms in $B_{12}N_{12}$.[32] Figure 1 illustrates the two lowest energy isomers. Both the isomers consist of six tetragonal rings and eight hexagonal rings and the carbon atoms form three B_2C_2 squares. The isomers (a) and (b) have C_3 and C_{2v} symmetry respectively, and their energy difference is only 0.04 eV. In $B_{12}C_6N_6$, the highest occupied molecular orbital (HOMO) is mainly composed of 2p orbitals of B and C and the lowest unoccupied molecular orbital (LUMO) is dominated by 2p orbital of C. In this electron deficient cage, the frontier molecular orbitals are formed by the partially occupied 2p orbitals of the unsaturated carbon atoms and they are highly delocalized. The electronic structure of the carbon sites is favourable for combining metal atoms.

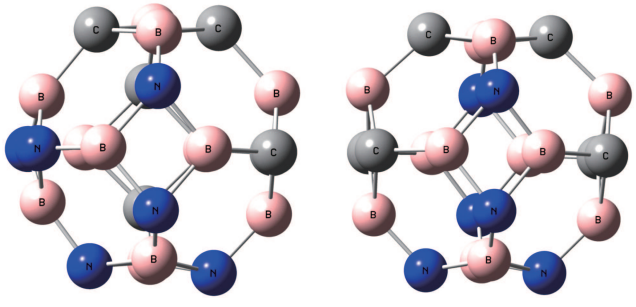


Fig. 1. (color online) Two lowest energy isomers of $B_{12}C_6N_6$.

3.2. Geometric structures of Mg-coated $B_{12}C_6N_6$

Firstly, we perform structure optimization for the Mg-coated clusters. In the initial structures, Mg atoms are placed on different sites of $B_{12}C_6N_6$, such as the tops of B, C, and N atoms, different BC and BN bridges, and above the nonequivalent rings. To judge the binding strength of Mg atoms, we define the average binding energy E_b as

$$E_b = [E(B_{12}C_6N_6Mg_n) - E(B_{12}C_6N_6) - nE(Mg)]/n,$$

where $E(B_{12}C_6N_6Mg_n)$ is the total energy of the Mg-coated clusters, $E(B_{12}C_6N_6)$ is the energy of $B_{12}C_6N_6$, and $E(Mg)$ is the energy of the isolated Mg atom. The most stable configurations of $B_{12}C_6N_6Mg_n$ are shown in Fig. 2, and the values of average binding energy E_b are given in Table 1. When a single Mg atom is coated, the strongest binding site is above the B_2C_2 square. In the case of coating two Mg atoms, the optimization shows that the configurations having two Mg atoms on the same B_2C_2 square are more stable than those having two Mg atoms seperated. When coating three Mg atoms, the Mg atoms are located above three different B_2C_2 squares. For coating six Mg atoms, the three paires of Mg atoms binding on the three B_2C_2 squares are very stable, and the binding energies on isomers (a) and (b) are close.

In Table 1 there are listed the average distances from Mg to the close B and C atoms. The geoemtries of (a)&Mg_1 and (b)&Mg_1 are slightly deformed; the carbon atoms in the B_2C_2 square move toward the Mg atom. The distances between Mg–B atoms are 2.25 Å/2.27 Å and the distance between Mg–C is 2.12 Å. When coating a pair of Mg atoms on the B_2C_2 square, the Mg atoms combine with the C atoms ((a)&Mg_2, (a)&Mg_6, (b)&Mg_2, (b)&$Mg_{2'}$, (b)&Mg_6), and the distances of d_{Mg-C} and d_{Mg-B} are in the ranges of 2.10 Å–2.13 Å and 2.87 Å–2.93 Å respectively. The binding energies in Table 1 show that the binding in (b)&Mg_1 is strongest, and the binding energy is −1.90 eV. The average binding energy in (a)&Mg_2 is the same as the value in (a)&Mg_1. The binding energy in (b)&Mg_2 is −1.69 eV; it is weaker than that in (b)&Mg_1 but still stronger than those in (a)&Mg_1 and (a)&Mg_2. The average binding energies for coating six Mg atoms are −1.50/ − 1.52 eV. The binding is weaker than those of coating one and two Mg atoms, but it is obviously stronger than the binding of coating three Mg atoms. According to the stability of the Mg-coated clusters, we will study in detail the adsorption and dissociation of hydrogen molecule on (b)&Mg_1, (a)&Mg_1, and (a)&Mg_2.

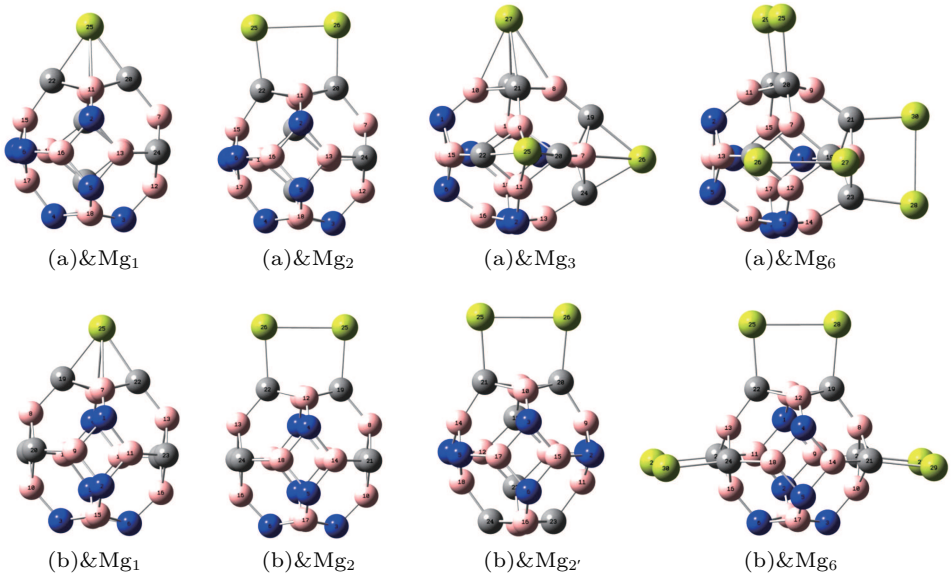


Fig. 2. (color online) Optimized configurations of Mg-coated $B_{12}C_6N_6Mg_n$. The preferred binding sites for Mg atom are the B_2C_2 rings.

Table 1. Values of average bond length (in unit Å) of Mg–B, Mg–C, and the average binding energy E_b (in unit eV) per Mg atom.

System	d_{Mg-B}/Å	d_{Mg-C}/Å	E_b/eV
(a)&Mg_1	2.25	2.12	–1.62
(a)&Mg_2	2.90	2.12	–1.62
(a)&Mg_3	2.41	2.23	–1.14
(a)&Mg_6	2.87	2.11	–1.50
(b)&Mg_1	2.27	2.12	–1.90
(b)&Mg_2	2.93	2.13	–1.69
(b)&$Mg_{2'}$	2.88	2.11	–1.53
(b)&Mg_3	2.25	2.11	–1.31
(b)&Mg_6	2.87	2.10	–1.52

3.3. Electronic structure of Mg-coated $B_{12}C_6N_6$

The total and partial density of states (DOS) of the pristine and Mg-coated $B_{12}C_6N_6$ clusters are presented in Fig. 3. The energy levels are represented by Gaussian distributions with a half width of 0.4 eV. In the pristine $B_{12}C_6N_6$(a), the doubly degenerated HOMO is located at −6.94 eV, the triply degenerated LUMO is located at −3.73 eV, and it is formed by C 2p. When we coat one Mg atom on it, the HOMO at −5.80 eV is formed by C 2p, the LUMO at −3.88 eV is formed by Mg 3s, and the LUMO+1 and LUMO+2 are still formed by C 2p. It means the Mg atom transfers its two valence electrons to the unoccupied C 2p orbitals of $B_{12}C_6N_6$, and the 3s orbital of Mg is left unoccupied. Similarly, the Mg atom transfers the 3s electrons to the C 2p orbitals in (b)&Mg_1; the HOMO at −5.65 eV is formed by C 2p and the LUMO located at −3.84 eV is formed by Mg 3s. When two Mg atoms are coated on $B_{12}C_6N_6$(a), the Mg atoms transfer two electrons to the C 2p orbitals and form the HOMO–1 at −6.12 eV, the HOMO at −5.55 eV is formed by Mg 3s orbitals. Analyses of the molecular orbitals show that the 3s orbitals of the two Mg atoms form one bonding orbital (the HOMO) and one antibonding orbital (the one at −2.90eV). There are still two unoccupied C 2p orbitals (at −3.13 eV and −2.67 eV). While two Mg atoms are coated on $B_{12}C_6N_6$(b), two electrons transfer from Mg 3s to C 2p and form the HOMO-1 at −5.69 eV, and two electrons remain in the bonding orbital formed by Mg 3s. The LUMO at −2.92 eV is the antibonding orbital formed by Mg 3s, and the two unoccpuied orbitals formed by C 2p are located at −2.36 eV and −2.02eV, respectively. For the configuration (a)&Mg_3, four electrons of Mg atoms transfer to the C 2p orbitals (−5.54 eV and −5.78 eV). The 3s orbitals of Mg atoms form three delocalized orbitals; one is the HOMO and the other two are located at −3.52 eV and −3.41 eV, respectively. When coating six Mg atoms on $B_{12}C_6N_6$, the 3s orbitals of the three paires of Mg atoms form three bonding orbitals (the doubly degenerated orbitals at −4.89 eV and the orbital at −5.15 eV) and three degenerated antibonding orbitals (at −2.43 eV). Six electrons of Mg atoms transfer to the C 2p orbitals and six electrons occupy the three bonding orbitals formed by Mg 3s. The three degenerated antibonding orbitals form the LUMO. Now, the (a)&Mg_6 forms a perfect closed electronic shell after all of the bonding orbitals have been filled. The HOMO–LUMO gap is 2.46 eV.

Table 2. HOMO, LUMO levels and values of energy gap E_g (in unit eV) of $B_{12}C_6N_6Mg_n$.

Systems	HOMO	LUMO	E_g
(a)&Mg_1	–5.80	–3.88	–1.92
(a)&Mg_2	–5.55	–3.13	–2.42
(a)&Mg_3	–4.19	–3.52	–0.67
(a)&Mg_6	–4.89	–2.43	–2.46
(b)&Mg_1	–5.65	–3.84	–1.80
(b)&Mg_2	–5.54	–2.92	–2.62
(b)&$Mg_{2'}$	–5.70	–3.26	–2.44
(b)&Mg_3	–4.65	–3.30	–1.35
(b)&Mg_6	–4.76	–2.46	–2.30

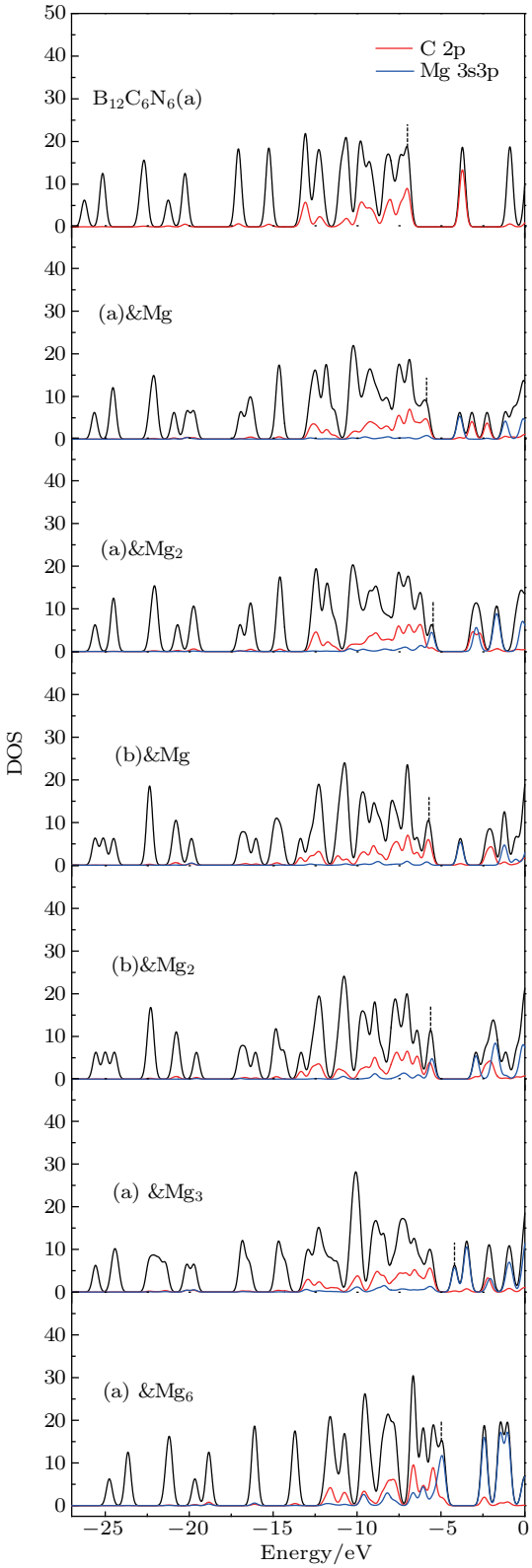


Fig. 3. (color online) Total and partial density of states of the pristine and Mg-coated $B_{12}C_6N_6$ cages. The red line denotes the partial density of C 2p and the blue lines refers to Mg 3s3p. The HOMO levels are marked with dash lines

3.3.1. Molecular and dissociated adsorption of H_2 on Mg-coated $B_{12}C_6N_6$

The configurations of H_2 molecule adsorbed on Mg-coated $B_{12}C_6N_6$ are optimized by B3LYP/6-31G(d,p). We take into account the different orientations of H_2 molecule in the initial structures. Figure 4 illustrates the stable configurations of H_2 adsorbed systems ((b)&Mg_1–H_2, (a)&Mg_1–H_2, and (a)&Mg_2–H_2). The optimization shows that the H_2 molecule is adsorbed at the top of the Mg atom in the side-on manner. To measure the strength of H_2 adsorption, the adsorption energy E_{ad} is defined as

$$E_{ad} = E(B_{12}C_6N_6Mg_n{-}H_2) - E(B_{12}C_6N_6Mg_n) - E(H_2),$$

where $E(B_{12}C_6N_6Mg_n{-}H_2)$ is the total energy of the H_2 adsorbed complexes, $E(B_{12}C_6N_6Mg_n)$ is the energy of Mg-coated $B_{12}C_6N_6$, and $E(H_2)$ is the energy of isolated H_2 molecule. The H–H distance of free H_2 is nearly preserved in the adsorption states. The adsorption energies of (b)&Mg_1–H_2 and (a)&Mg_1–H_2 are -0.17 eV and -0.19 eV respectively. These results show that Mg^{2+} produces a strong local electric

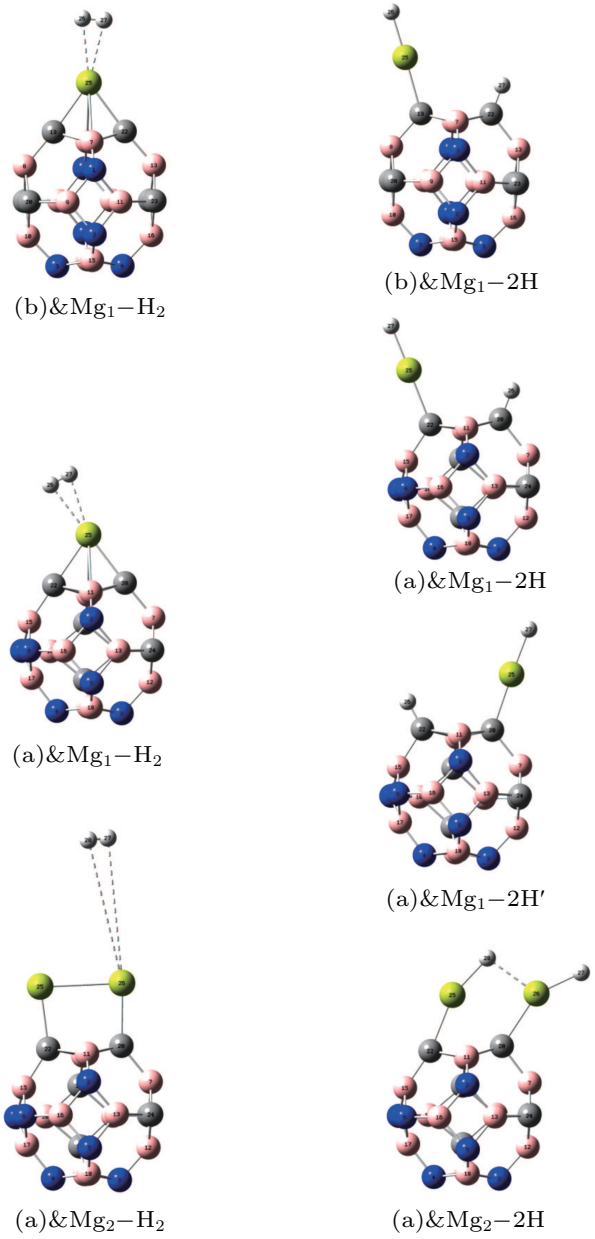


Fig. 4. (color online) Optimized configurations of the H_2 adsorbed systems and the dissociation products.

field and the H_2 molecule is moderately polarized. Therefore, there is a strong electrostatic interaction between hydrogen molecule and the cluster. The adsorption of H_2 molecule on cluster (a)&Mg_2/(b)&Mg_2 is very weak. The distances from H_2 to the Mg atoms are around 7 Å, and the adsorption energies are about −0.01 eV.

In order to investigate the dissociation processes of H_2 molecule on Mg-coated $B_{12}C_6N_6$, we firstly determine the stable dissociation products. We carry out a series of calculations by elongating the H–H distance in the H_2-adsorbed configurations to find the dissociation configurations. We also optimize the configurations of adsorbing two hydrogen atoms on different pairs of Mg and other atoms. The most stable configurations of H_2 dissociated on (b)&Mg_1, (a)&Mg_1, and (a)&Mg_2 are also presented in Fig. 4. For the dissociations on (b)&Mg_1 and (a)&Mg_1, two hydrogen atoms are adsorbed on the tops of Mg and C atoms in the B_2C_2 ring. For the dissociation on (a)&Mg_1, there are two stable structures: (a)&Mg_1–2H and (a)&Mg_1–2H′. The former configuration is 0.04 eV lower in energy. In the following sections, we will investigate the dissociation processes leading to these four dissociation products (b)&Mg_1-2H, (a)&Mg_1–2H, (a)&Mg_1–2H′, and (a)&Mg_2–2H.

3.3.2. Dissociation process of H_2 on (b)&Mg_1

In order to obtain the transition state (TS) of the dissociation process, we perform a series of partial optimization by turning the H_2 molecule towards the carbon atom. This is done step by step by setting the angle β (in Fig. 5) with different values. The optimization illustrates that the total energy of the system rises gradually while the β increases from the initial molecular adsorption state (b)&Mg_1–H_2 ($\beta = 149.3°$). The energy reaches the highest value around $\beta = 77.14°$ and then the H–H bond dissociates rapidly and the Mg atom moves to the top of one carbon atom. We carry out the TS optimization around $\beta = 77.14°$ and obtain the transition state TS1, in which the H–H distance is 0.86 Å. We then study the dissociation process by using the reaction path following algorithm, i.e., intrinsic reaction coordinate (IRC). The IRC calculations confirm that TS1 lies on the minimal energy pathway between the molecular adsorption state (b)&Mg_1–H_2 and the dissociation product (b)&Mg_1–2H. The energy curve along the dissociation path is shown in Fig. 5. The energies of the molecular adsorption state, the dissociation product and the transition state are listed in Table 4. The energy barrier for the dissociation is 0.21 eV. The energy barrier is much smaller than the dissociation energy of free H_2 molecule (The dissociation energy of a free H_2 is 4.48 eV[40]). Figure 5 also shows the molecular orbital dominated by the orbitals of hydrogen in the TS1. The orbital compositions show that the orbitals of H mix strongly with the 3s of Mg and 2p of C.

Table 3. NBO and AIM charges (in unit e) on Mg atoms in $B_{12}C_6N_6Mg_n$.

Systems	NBO	AIM
(a)&Mg_1	1.38	1.51
(a)&Mg_2	0.70/0.72	0.70/0.79
(a)&Mg_3	0.63/1.13/1.18	0.70/1.25/1.28
(a)&Mg_6	0.66–0.69	0.71
(b)&Mg_1	1.38	1.51
(b)&Mg_2	0.71	0.74
(b)&$Mg_{2'}$	0.73	0.76
(b)&Mg_3	1.30/1.32	1.44/1.46
(b)&Mg_6	0.67–0.69	0.71–0.73

Table 4. Energies (in unit eV) of the molecular adsorption states, dissociation products, and the transition states along the five dissociation paths.

Systems	Molecular adsorption	TS	Dissociation products
(b)&Mg_1–H_2	–0.17	0.04	–2.09
(a)&Mg_1–H_2	–0.19	0.02	–2.15
		–0.08	–2.11
(a)&Mg_2–H_2	–0.01	1.19	–0.86
(b)&Mg_2–H_2	–0.01	1.19	–0.90

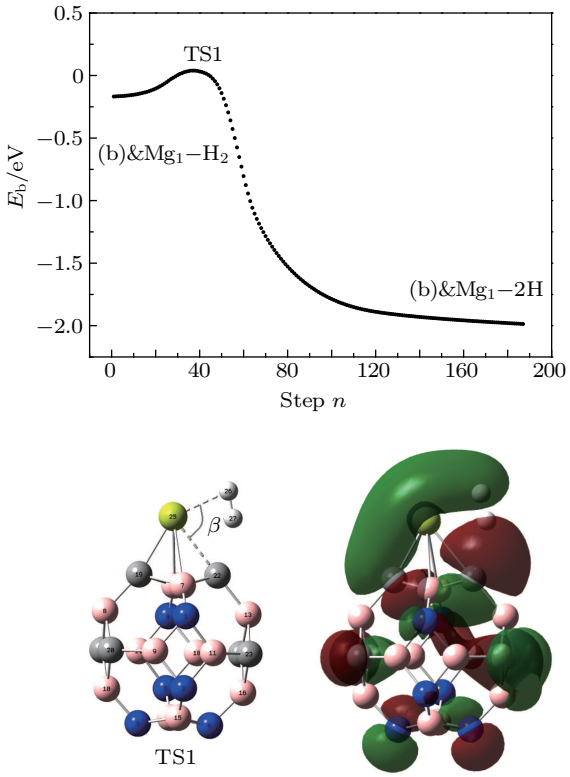


Fig. 5. (color online) Dissociation process of H_2 molecule starting from the molecular adsorption configuration (b)&Mg_1–H_2. The energies are given to be relative to the energy of $B_{12}C_6N_6$ and free H_2, and n represents the number of IRC steps. The molecular orbital dominated by the orbitals of hydrogen in TS1 is also presented.

3.3.3. Dissociation process of H_2 on (a)&Mg_1

The dissociation process starting from the molecular adsorption state (a)&Mg_1–H_2 is given in the following Fig. 6. When the H–H bond is stretched step by step, the partial

optimization (specifying H–H distance with different values) shows that the H_2 molecule moves to the right side and the total energy increases slowly. When the H–H distance exceeds 0.85 Å, the energy decreases rapidly and the H_2 molecule dissociates into (a)&Mg_1–2H. We carry out TS optimization with an initial H–H distance of 0.85 Å and obtain an accurate structure of TS2-1. The transition state TS2-2 is found by using the QST3 method. The QST3 algorithm determines the transition state structure based on the given reactant, product, and estimated TS configurations. After the transition states are determined, we perform the IRC calulations to follow the dissociation paths. Figure 6 shows the energy curves of the two dissociation processes. The energy barriers for the dissociation of H_2 along these two paths are 0.11 eV and 0.21 eV, respectively. We also optimized the molecular adsorbed configurations and the TS structures by making use of the mp2/6-31g(d,p) method, the energy barriers corresponding to TS1, TS2-1, and TS2-2 are 0.36 eV, 0.35 eV, and 0.27 eV respectively.

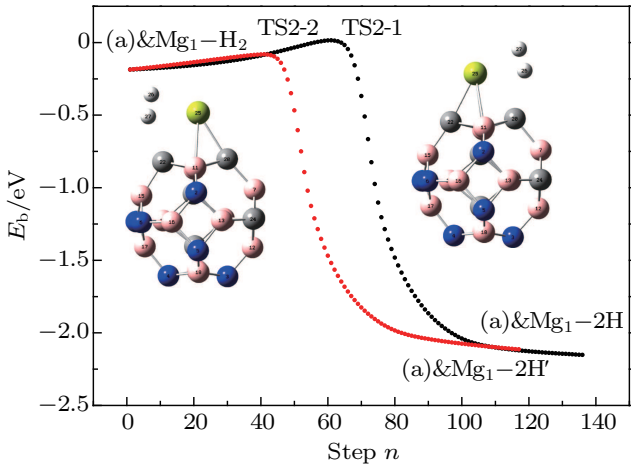


Fig. 6. (color online) Two dissociation processes of H_2 molecule starting from the molecular adsorption configuration (a)&Mg_1–H_2.

3.3.4. Dissociation process of H_2 on (a)&Mg_2

For the dissociation of H_2 on (a)&Mg_2, it can be easily studied step by step by specifying the H–H distance with different values. When the H–H bond is stretched, the total energy increases considerably. After passing through the transition state (at the H–H distance of 0.98 Å), the H–H bond dissociates and the energy drops rapidly. We also confirm the transition state TS3 by using the QST2 algorithm, which searches for the TS from the given reactant and product. The energy curve along the dissociation path calculated by IRC is given in Fig. 7. The energy barrier for the H_2 dissociation on (a)&Mg_2 is 1.19 eV. The high energy barrier shows that the Mg_2 pair is not suitable for dissociating the H_2 molecule.

4. Conclusions

By means of density functional theory computations, we investigate the adsorption and dissociation of H_2 on Mg-coated $B_{12}C_6N_6$. The results indicate that Mg atoms can be strongly bound to this electron deficient cage. At low doping density, single Mg atom can be bound to the B_2C_2 rings with binding energies over 1.6 eV. The DOS and NBO/AIM charges show that the Mg atoms transfer their 3s electrons to the virtual 2p orbitals of carbon in the cluster and exist with large positive charges. H_2 molecules can be moderately polarized by the Mg^{2+} ion, and the adsorption energies are close to −0.2 eV. The stable dissociation structures corresponding to each adsorption configuration are determined. We study the dissociation processes leading to the four most stable dissociation products; the transition states are carefully determined and the dissociation paths are traced by using the IRC algorithm. The results show that strong orbital interactions between the hydrogen and the cluster occur in the transition states, and the energy barriers for hydrogen dissociation over a single Mg atom range from 0.11 eV to 0.21 eV. It means that the H_2 molecules can be easily dissociated on Mg-coated $B_{12}C_6N_6$ at ambient temperature.

Acknowledgment

We thank the National Supercomputer Centre in Guangzhou and in Shenzhen for computation resources.

References

[1] Mazloomi K and Gomes C 2012 *Renew. Sust. Energ. Rev.* **16** 3024
[2] Züttel A, Remhof A, Borgschulte A and Friedrichs O 2010 *Phil. Trans. R. Soc. A* **368** 3329
[3] Lubitz W and Tumas W 2007 *Chem. Rev.* **107** 3900
[4] Yilanci A, Dincer I and Ozturk H K 2009 *Prog. Energ. Combust. Sci.* **35** 231
[5] Eisenberg R and Nocera D G 2005 *Inorg. Chem.* **44** 6799
[6] Momirlan M and Veziroglu T N 2002 *Renew. Sust. Energ. Rev.* **6** 141
[7] Graetz J 2009 *Chem. Soc. Rev.* **38** 73
[8] Xiong Z, Yong C K, Wu G, Chen P, Shaw W, Karkamkar A, Autrey T, Jones M O, Johnson S R, Edwards P P and David W I 2007 *Nat. Mater.* **7** 138
[9] Jena P 2011 *J. Phys. Chem. Lett.* **2** 206
[10] Principi G, Agresti F, Maddalena A and Russo S L 2009 *Energy* **34** 2087
[11] Schlapbach L and Züttel A 2001 *Nature* **414** 353
[12] Eberle U, Felderhoff M and Schüth F 2009 *Angew. Chem. Int. Ed.* **48** 6608
[13] Mandal T K and Gregory D H 2009 *Annu. Rep. Prog. Chem. Sect. A: Inorg. Chem.* **105** 21
[14] Suh M P, Park H J, Prasad T K and Lim D W 2012 *Chem. Rev.* **112** 782
[15] Ruan W, Wu D L, Luo W L, Yu X G and Xie A D 2014 *Chin. Phys. B* **23** 1296
[16] Jain I P, Lal C and Jain A 2010 *Int. J. Hydrogen Energy* **35** 5133
[17] Vegge T, Hedegaard-Jensen L S, Bonde J, Munter T R and N?rskov J K 2005 *J. Alloys Compd.* **386** 1
[18] Bhihi M, Lakhal M, Labrim H, Benyoussef A, El Kenz A, Mounkachi O and Hlil E K 2012 *Chin. Phys. B* **21** 097501

[19] Shevlin S A and Guo Z X 2009 *Chem. Soc. Rev.* **38** 211
[20] Norberg N S, Arthur T S, Fredrick S J and Prieto A L 2011 *J. Am. Chem. Soc.* **133** 10679
[21] Bérubé V, Radtke G, Dresselhaus M and Chen G 2007 *Int. J. Energy Res.* **31** 637
[22] Zhu Y, Li Y C and Wang F H 2016 *Acta Phys. Sin.* **65** 056801 (in Chinese)
[23] Ismail M, Zhao Y, Yu X B and Dou S X 2011 *Rsc Adv.* **1** 408
[24] Dehouche Z, Peretti H A, Hamoudi S, Yoo Y and Belkacemi K 2008 *J. Alloys Compd.* **455** 432
[25] Liu C S and Zeng Z 2010 *Appl. Phys. Lett.* **96** 123101
[26] An H, Liu C S, Zeng Z, Fan C and Ju X 2011 *Appl. Phys. Lett.* **98** 173101
[27] Deng Q M, Zhao L, Luo Y H, Zhang M, Zhao L X and Zhao Y 2011 *Nanoscale* **3** 4824
[28] Ye X J, Liu C S, Jia R, Zeng Z and Zhong W 2013 *Phys. Chem. Chem. Phys.* **15** 2507
[29] Gao Y, Wu X and Zeng X C 2014 *J. Mater. Chem. A* **2** 5910
[30] Wu X, Gao Y and Zeng X C 2008 *J. Phys. Chem. C* **112** 8458
[31] Qi P T and Chen H S 2015 *Acta Phys. Sin.* **64** 238102 (in Chinese)
[32] Li F, Zhang Y and Chen H 2014 *Physica E* **56** 216
[33] Jin X, Yang H, Zhang Y and Chen H 2015 *Int. J. Hydrogen Energy* **40** 16347
[34] Becke A D 1993 *J. Chem. Phys.* **98** 5648
[35] Lee C, Yang W and Parr R G 1988 *Phys. Rev. B* **37** 785
[36] Foresman J B, Ortiz J V, Cioslowski J, *et al.* 2009 Gaussian 09 Revision D.01 Inc. Wallingford, CT
[37] Reed A E, Weinstock R B and Weinhold F 1985 *J. Chem. Phys.* **83** 735
[38] Bader R F W 1991 *Chem. Rev.* **91** 893
[39] Lu T and Chen F 2012 *J. Comput. Chem.* **33** 580
[40] Herzberg G 1970 *J. Mol. Spectrosc.* **33** 147